Contract No.:

This manuscript has been authored by Battelle Savannah River Alliance (BSRA), LLC under Contract No. 89303321CEM000080 with the U.S. Department of Energy (DOE) Office of Environmental Management (EM).

Investigating the Role of Silver Oxidation State on the Thermodynamic Interactions between Xenon and Silver Functionalized Zeolites

*Kaitlin J. Coopersmith,[*a]† Katherine L. Broadwater,[a] Steven M. E. Demers,[a] Rebhadevi Monikandan,[b] Michael Torcivia,[a] Lindsay Roy,[a] and Douglas Hunter[a]*

a. Savannah River National Laboratory, P.O. Box A, Aiken, SC 29808, USA

b. Georgia Institute of Technology, Atlanta, GA 30332, USA

ABSTRACT

The molecular level understanding of the strong adsorption of Xe to silver modified zeolites remains elusive. Here, we probe the effect of silver oxidation state on the thermodynamics of Xe sorption in silver functionalized zeolites by measuring the enthalpies of adsorption after various treatments using inverse gas chromatography (IGC). The enthalpy of adsorption was measured for silver functionalized chabazites (AgCHA) before and after hydrogen reduction and subsequent re-oxidation. The sorption enthalpy (ΔH) for AgCHA was 35.2 kJ/mol which decreased to 25.8 kJ/mol with hydrogen reduction. After re-oxidation (O_2-AgCHA), 95% of the binding strength was restored. Hydrogen reduction of the base chabazite (CHA) did not influence Xe adsorption. Henry's law constant for Xe adsorption increased in the order AgCHA>O_2-AgCHA>H_2-AgCHA>CHA. A decrease in enthalpy and Henry's constant with silver reduction and increase with re-oxidation suggest that ionic silver is playing a role in Xe binding. The effect of reduction and re-oxidation on the zeolite microstructure was analyzed using surface area analysis, powder X-ray diffraction (p-XRD), scanning electron microscopy/electron x-ray spectroscopy

(SEM/EDS) and x-ray photoelectron spectroscopy (XPS). These results lay the groundwork for better material design of strong noble gas adsorbents.

INTRODUCTION

The efficient capture and release of noble gases from air remains both a technological and economical challenge with important applications in waste gas treatment,[1] detection of radioisotopes,[2] and industrial purification.[3,4] Radioactive Xe is formed in the fission of heavy elements and can be used for verification of the Comprehensive Nuclear Test Ban Treaty (CTBT).[2,5,6] Monitoring Xe isotopic ratios can discriminate nuclear tests from other sources, such as fuel reprocessing and research applications. Noble gases are important to nuclear monitoring due to their chemical inertness and gaseous state that allow for their atmospheric release; however, these same properties also make their detection and capture challenging.[5] In industrial applications, noble gases are collected and then separated through cryogenic separation, which is both time and energy intensive.[7] To overcome this, selective adsorbents can be employed that have high selectivity for different gases. Zeolites are one such highly microporous example and have been found to be one of the most selective materials for Xe,[8-19] Ar,[20,21] Kr,[22] and I_2[23] capture. Unlike metal organic frameworks (MOFs), zeolites maintain a stable state even in the presence of high radioactivity, high temperatures, and humid environments. Additionally, zeolites are reported to have significantly higher heats of adsorption than silver modified MOF's.[16,26]

Despite the large amount of research on Ag-zeolites as catalysts and gas adsorbents, the role of the silver atom on noble gas adsorption remains a complex issue with several contradictory reports in the literature.[9-14,16,17] There are many unknowns related to the role of silver on Xe capture, including the electronic state of silver. The literature reports are in disagreement whether the Ag^+

ions are responsible for Xe adsorption through d_π-d_π back-donation, through σ donation from the 5p orbital of Xe to the 5s orbital of Ag, whether Ag^0 or Ag^+ clusters are responsible,[13] or whether there is a chemical basis to the interaction at all (i.e. physisorption rather than chemisorption). CHA based zeolites were found to have a high affinity for Xe and is attributed to a close match between the size of the Xe atom and the CHA pore structure.[24] A formation of a partial bond between Xe atom and cation by donation of the Xe 5p electrons to the s-orbitals was proposed using ^{129}Xe NMR, where there were large paramagnetic contributions to the chemical shift of Xe gas.[9] ^{129}Xe NMR show there are different binding sites for Xe in silver zeolites.[25] In metal organic frameworks, an increase in polarizable halogenated functional groups led to an increase in gas uptake.[26]

The reduction of metal cations in ion exchanged zeolites has been investigated using a variety of optical spectroscopy and X-ray diffraction to determine the structure of the metal ions in the pores.[27,28] Baba, *et. al.* report that silver ions can be reversibly reduced from Ag^+ to Ag metal particles in Ag-Y zeolites. This reversible reduction, however, was dependent on the amount of reduction and the number of reduction/oxidation cycles to which the samples were exposed.[27] Partial reduction of AgCHA is hypothesized to cause Ag^+ ions in the pores to agglomerate and form silver clusters in the zeolite channels.[28] This could have an impact on Xe binding and retention, especially with possible silver migration and formation of clusters that may not have as strong of an interaction with Xe. Here, we aim to investigate the role that the silver plays in the strong noble gas sorption in zeolites.

In this work, enthalpies of adsorption (ΔH) and Henry's Law constants were measured using inverse gas chromatography (IGC) for Xe sorption in silver modified chabazites (AgCHA).[29] The specific retention time of Xe was measured as a function of temperature before and after reduction

(H_2-AgCHA) and re-oxidation (O_2-AgCHA) of the silver modified zeolites. IGC allows the measurement of surface properties in a chromatographic column packed with the sorbent under investigation.[30,31] The silver modified zeolite was packed into the column and measured at low Xe concentrations at different temperatures. The zeolite was then reduced and subsequently re-oxidized to investigate the effect of the oxidation state on the sorbent properties.

EXPERIMENTAL

Materials

Ultra-high purity (UHP) Helium, UHP Argon, Research grade Xe, and Oxygen (20% O_2/He) and Hydrogen mixtures (3% H_2/He) were purchased from Nexair. Silver nitrate was purchased from Sigma Aldrich. Synthetic chabazite (IONSIV R9160, Honeywell) was used in this work. Chabazites have a general formula $M_2[Al_2Si_4O_{12}]_2$ where M=Na, K, Ca, or Mg framework ions that balance out the ionic charge.

Characterization

X-Ray Photoelectron spectroscopy (XPS). Measurements were obtained on Thermo K alpha XPS using mono-chromated Al-Kα X-rays with 200 μm x-ray spot size. The instrument was calibrated with Cu 2p, Ag 3d and Au 4f internal standards. Samples were loaded into a powder sample holder and evacuated for 1.5 hours before transferring to the analysis chamber. Etching was carried out with Ar ion gun at 500-2000 eV and 30-90 s etch times per level on 1x2mm spot size. All peaks were fitted with best fit peaks to establish the peak positions.

Powder X-Ray Diffraction (p-XRD). Crystallographic measurements were collected on a Rigaku Ultima IV diffractometer with Cu-Kα radiation (40 kV, 44 mA, λ=1.5418 Å) and a scanning step size of 0.01° using a d/tex detector and CBO optics. Silver reference pattern was

obtained through ICDD (PDF 00-003-0921) and the chabazite reference pattern was obtained from a previously reported simulated chabazite spectrum.[32]

Scanning Electron Microscopy and Energy Dispersive X-ray Spectrometry (SEM/EDX). SEM/EDX measurements were carried out on a SU8230 SEM (Hitachi) equipped with an X-Max 150 Silicon Drift Detector.

Gas Characterization. Temperature programmed reduction (TPR) and surface area analyses were measured on an Anton Paar Quantachrome Autosorb iQ analyzer equipped with a thermal conductivity detector (TCD). Prior to analysis, samples were outgassed at 300°C for 300 minutes. After outgassing, samples were tested for the presence of residual water by monitoring the sample for pressure rise at 300°C ($\Delta P<25$ mTorr). Surface area analyses were carried out using nitrogen adsorption-desorption isotherms at 77K. Surface area and pore sizes were calculated using the DFT method. Temperature programmed reduction experiments were carried out with 3% H_2/He. The temperature programmed reduction (TPR) of the different zeolites was carried out to verify reduction of the CHA and AgCHA (Figure S1). The reduction experiments in the following reactions were carried out at 300 °C for 4 hours, conditions where both the CHA and AgCHA samples are reduced.

Gas Chromatography (GC). GC measurements were carried out on Perkin Elmer Clarus GC equipped with a TCD. U loop GC columns were made with 1/4" inch stainless steel tubing and were packed with about 2 g of zeolites. The samples were outgassed at 300°C overnight to remove adsorbed water using the same procedure as the surface area analysis. UHP He was used as the carrier and TCD reference gas and flowed through the column at 10 mL/min. The flow rate was measured before each experiment to ensure consistent flow rate through the column and the TCD.

The injector port was held at 175°C and the TCD was maintained at 300°C. Thermodynamic measurements were carried out isothermally.

Silver Modification. Zeolites were functionalized with silver by incubation at room temperature with 0.1 M $AgNO_3$ solution for 24 hours in the dark. The zeolites were purified and cleaned with fresh deionized water under vacuum filtration. The final silver modified zeolites (Ag-CHA) were dried in an oven overnight at 125°C. The average silver loading was measured in triplicate on SEM/EDS as 10.8±1.7 wt%. The M:Si:Al atomic ratio was measured as 0.8:1:2.8 from SEM/EDS, where M=Na, K, and Ca.

Zeolite Treatment. An overview of the samples prepared for this work is found in Table 1. Treatment of AgCHA samples were carried out with a heat ramp of 10°C/min and a flow rate of 20 mL/min. The samples were exposed to the different gases for 300 mins.

Table 1. Sample nomenclature and preparation method for these experiments.

Sample	Treatment
CHA	Base chabazite (sodium based)
H_2-CHA	Reduction of base chabazite at 300 °C with hydrogen (3% H_2/He)
AgCHA	Chabazite after silver ion exchange
H_2-AgCHA	Reduction of silver chabazite at 300 °C with hydrogen (3% H_2/He)
O_2-AgCHA	Re-oxidation of Ag-CHA at 300 °C with oxygen (20% O_2/He)

Thermodynamic Measurements. Xe was injected at infinite dilution conditions, where interaction with lower energy sites are negligible and the interactions are assumed to only occur

with the high-energy sites on the surface.[30] This is confirmed by the constant retention time that was independent of volume, and a linear adsorption region (Figure S1). Henry's Constant (K) was calculated from the mass flow rate (Q), net retention time ($V_R = t_{Xe}-t_0$) between the retention time of Xe (t_{Xe}) and the retention time of nitrogen (t_0), gas constant (R), column temperature (T), and mass of the zeolite in the column (m) as shown in equation (1):

$$K=\frac{V_R Q}{mRT} \quad (1)$$

The enthalpy of adsorption (ΔH) was experimentally determined as the slope from a plot of ln(K) and -1/RT using equation (2):

$$\ln(K) = -\frac{\Delta H}{RT} + C \quad (2)$$

Where C is the constant containing entropy information. All samples were run in triplicate at each temperature and regenerated between each run by ramping the temperature to 320 °C and heating for 60 minutes.

RESULTS & DISCUSSION

Zeolites were loaded into a GC column to measure the thermodynamics of noble gas adsorption. Figure 1 shows the gas chromatogram for Xe injected into columns packed with unmodified chabazites (CHA) and silver modified chabazites (AgCHA). The GC trace for the AgCHA shows a longer retention time for Xe compared to the CHA sample, indicating a stronger interaction with the AgCHA. These injections were carried out at volumes where the Xe retention time (t_{Xe}) is independent of injected volume, which occurs at conditions of infinite dilution (Figure S2). These experiments were carried out with 40 μL of injected Xe; however, previous reports measure high isoteric heats of adsorption of Xe in AgCHA even at atmospheric levels (below 1 ppm).[13]

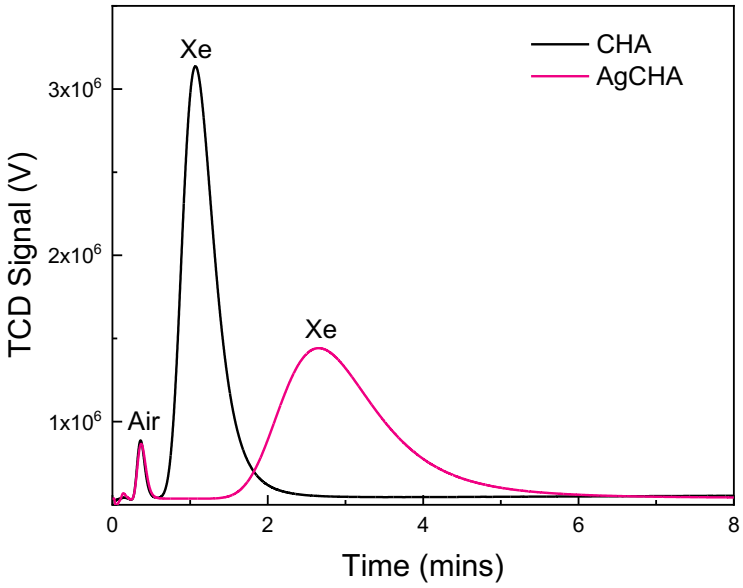

Figure 1. Gas chromatogram for a 40 µL Xe injection in column packed with different zeolites injected at 200 °C. The elution centered at 1 min for CHA is pushed outward to 2.5 min for AgCHA.

To investigate the role of the oxidation state of silver on the thermodynamic measurements, CHA and AgCHA were reduced with 3% H_2/He and then re-oxidized with 20% O_2/He (Figure 2). Xe adsorption was measured after each gas treatment.

Figure 2. Reduction and oxidation of AgCHA to investigate the role of oxidation state on Xe adsorption

Thermodynamic parameters after Xe adsorption were calculated from isothermal GC/TCD measurements (Figure 3 and Figure 4). Reduction led to a change in Xe retention time and peak shape for the AgCHA sample but not for the unmodified zeolites (CHA), as shown in Figure 3. After hydrogen reduction for the AgCHA sample, the GC peak was narrower, indicating a decrease in binding to the sample. With re-oxidation (O_2-AgCHA), the retention time shifted back towards the AgCHA peak. The GC peak for the O_2-AgCHA is not overlapping completely with the AgCHA, possibly due to incomplete oxidation of the zeolites. the presence of irreversibly reduced silver particles, or blocked pores from silver aggregates that may have formed during the reduction and re-oxidation process.[28]

In summary, the strength of Xe adsorption increased in the order CHA>H_2-AgCHA>O_2-AgCHA>AgCHA. This indicates the affinity between Xe and the zeolites decreased with hydrogen reduction and increased with re-oxidation and that the charge and microstructure of the silver in the zeolite plays a major role in the strength of Xe adsorption. The H_2-AgCHA sample had stronger thermodynamic interactions than the unmodified CHA, indicating that this adsorption is due to the interaction between Xe and silver. Since the AgCHA had the strongest thermodynamic interactions with the Xe, it is hypothesized that silver in the positively charged state (i.e. Ag^+ ions or clusters) have the strongest affinity for Xe adsorption. Xe adsorption increased with decreasing temperature as indicated by longer retention times and broader peaks.

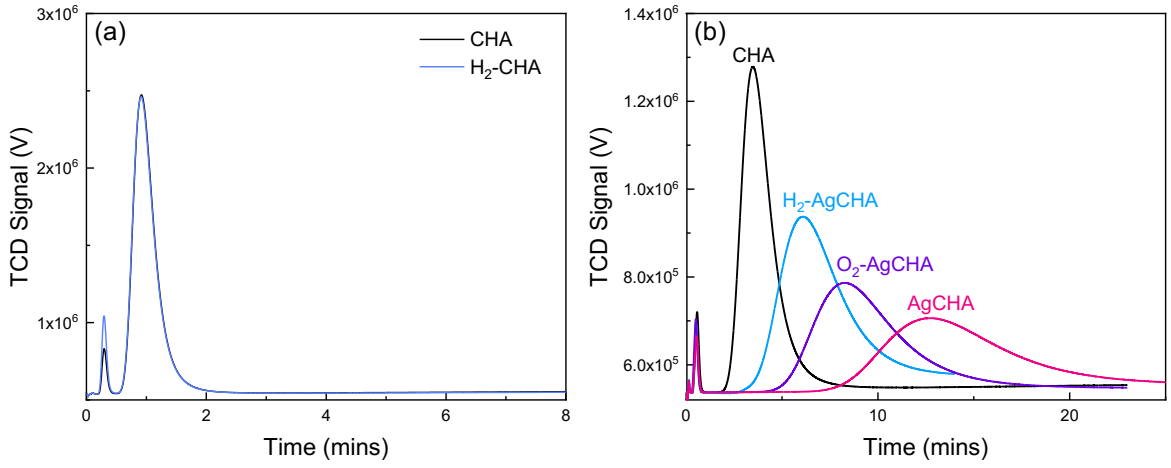

Figure 3. Effect of reduction and reoxidation on Xe elution at 200 °C for (a) CHA and (b) AgCHA.

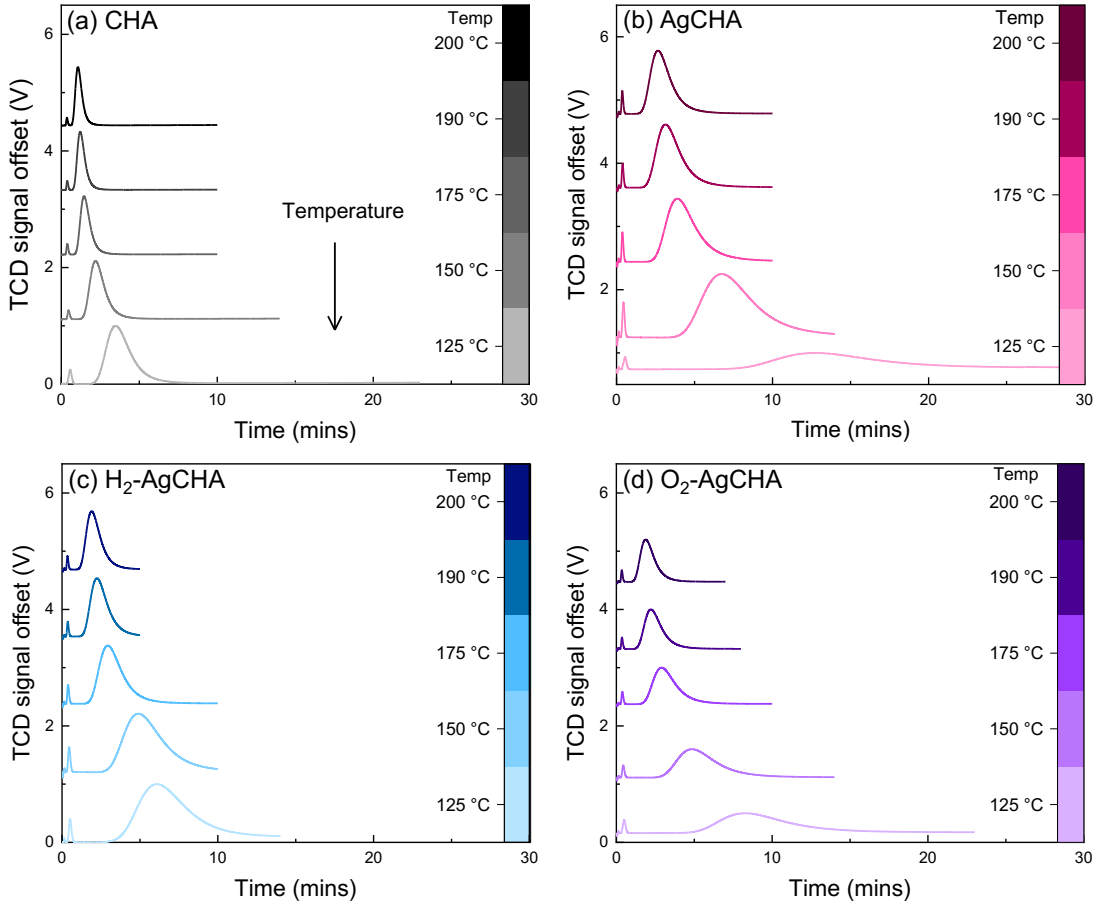

Figure 4. Isothermal spectra of Xe injections for different samples: (a) CHA, (b) AgCHA, (c) H_2-AgCHA, (d) O_2-AgCHA. All peaks are normalized to the Xe peak intensity.

The interaction energies between Xe and AgCHA were calculated from retention times as a function of inverse temperature. As shown in Figure 5a, AgCHA had the ability to retain significant amounts of Xe, with isosteric heat of adsorption of 35.2 kJ/mol. This comparable to other reported heats of adsorption for Xe adsorption to zeolites.[16, 24]

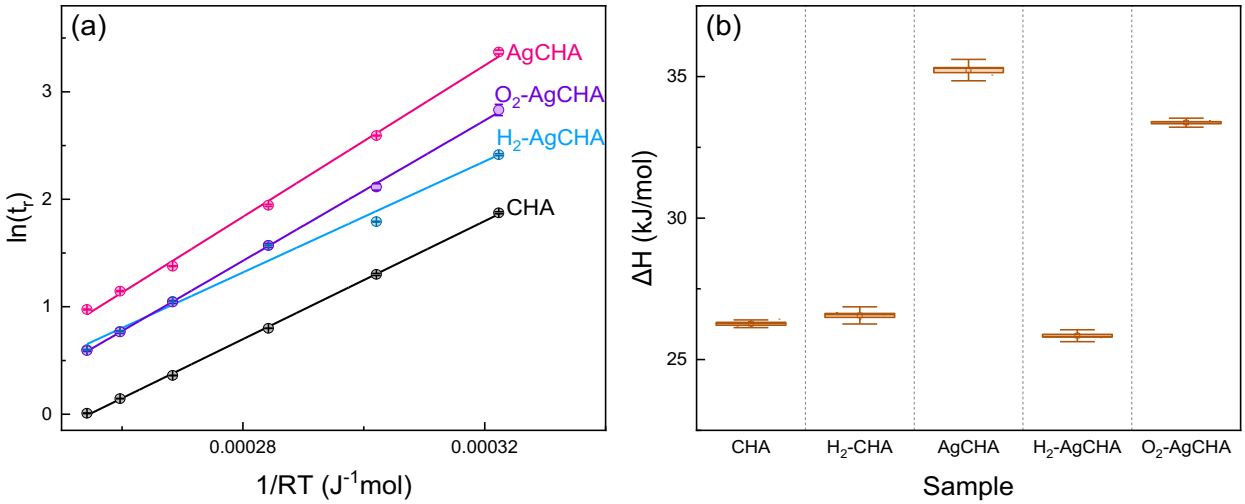

Figure 5. (a) Retention time vs inverse temperature plots for the different Ag-CHA samples; the slope of the line gives the heat of adsorption; (b) effect of zeolite treatment on the heat of adsorption for Xe; box indicates standard error of measurement, and the whisker shows 5-95 percentile.

Reduction of the zeolites with hydrogen and subsequent reoxidation with oxygen led to significant changes in the heats of adsorption, as shown in Figure 5b. The heat of adsorption decreased from AgCHA>O_2-AgCHA>H_2-AgCHA=H_2-CHA=CHA. The ΔH for the H_2-AgCHA was the same as CHA within error. Re-oxidation of the zeolites led to almost complete recovery (95%) of the ΔH before any reduction. Reduction of the base chabazite without silver (CHA) also didn't have an effect, indicating that hydrogen is not affecting the base zeolite. Since reduction

had a significant effect on the AgCHA and not CHA, the change in the oxidation state of silver plays a significant role in the thermodynamic adsorption of Xe. Temperature programmed desorption experiments (TPD) with Xe on AgCHA, H_2-AgCHA and CHA show similar results to the GC measurements. As shown in Figure S3, the desorption of Xe is reduced in the H_2-AgCHA sample as compared to the AgCHA samples. It is hypothesized that silver nanoparticles hinder Xe adsorption to the zeolites, since previous work has shown that hydrogen reduction of the silver cations in chabazites leads to the formation of silver nanoparticles.[27,33,34]

Henry's Law constant (K) was calculated for each sample and is found in Table 2. K decreases in the following order: AgCHA>O_2-AgCHA>H_2-AgCHA>CHA. Henry's law constant is directly proportional to the solubility of the gas in a solid, therefore the constant can give an indication of the relative number of binding sites for the different samples.[35] At 100 °C, the K for AgCHA sample was 4.5 times larger than CHA, 2.4 times larger than H_2-AgCHA and 1.5 times larger than O_2-AgCHA. This indicates that almost 65% of the adsorption was recovered with oxidation and may be further increased with increased exposure to O_2. This is consistent with the mass adsorbed at 100 °C. The AgCHA sample adsorbed 0.044 μg Xe/g zeolite, the H_2-AgCHA adsorbed 0.008 μg/g, and O_2-AgCHA adsorbed 0.03 μg/g, which is a 63% recovery of Xe adsorption for the O_2-AgCHA compared to the AgCHA.

Table 2. Calculated Henry's Law Constants (K) for the different samples

Sample	**K ($mol \cdot kg^{-1} \cdot kPa^{-1}$)**					
	100°C	**125°C**	**150°C**	**175°C**	**190°C**	**200°C**
CHA	0.0103	0.00561	0.00329	0.00205	0.00162	0.00139
AgCHA	0.0464	0.0204	0.0102	0.00557	0.00430	0.00356
H_2-AgCHA	0.0192	0.00967	0.00729	0.00408	0.00299	0.00247
O_2-AgCHA	0.0299	0.0134	0.00735	0.00411	0.00302	0.00249

To investigate the structural effects that occurred with reduction and oxidation, surface area measurements, p-XRD, and SEM/EDX measurements were carried out. Surface area measurements were obtained using nitrogen isotherms. As shown in Table 3, a decrease in surface area was observed with ion exchange. This is expected; however, since the surface area decreased with ion exchange while the Xe adsorption significantly increased, it is presumed the silver is playing a role in the Xe binding. For the unmodified zeolites, hydrogen reduction did not change the surface area significantly. The surface area is a balance between the formation of AgNPs on the surface and potential pore blocking effects from the movement of reduced Ag^0 atoms. The slight increase in surface area and micropore volume may be due to the removal of strongly bound water in the pores. This data suggests that the reduction did not significantly change the base chabazite pore structure. Reduction of the AgCHA did not change the surface area of the zeolite within error; however, reoxidation decreased the surface area significantly. Most of the Xe activity recovered after oxygen treatment, so the surface area does not appear to correlate with Xe adsorption. This may point towards a chemical, rather than physical, mechanism of adsorption.

Table 3. Surface area analysis from nitrogen isotherms at 77K

Sample	Surface Area (m^2/g)
CHA	451 ± 4
H_2-CHA	462 ± 19
AgCHA	400 ± 30
H_2-AgCHA	401 ± 29
O_2-AgCHA	292 ± 27

The microstructural effects of reduction and oxidation on the zeolites was measured using SEM/EDS. As shown in Figure 6 and Figure 7, the reduction led to the formation of silver particles, as confirmed by EDS (Figure 7). These particles were not visible on the SEM before reduction or after oxidation (Figure 6c).

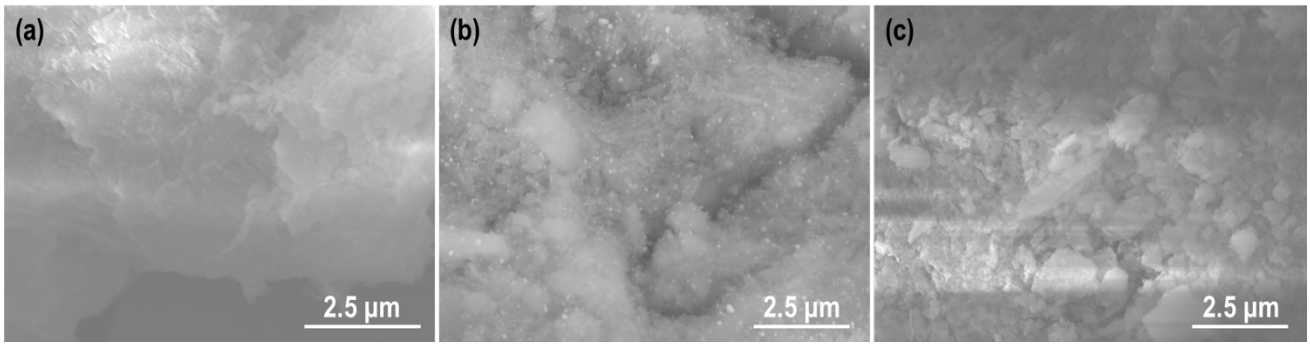

Figure 6. SEM images for (a) AgCHA, (b) H_2-AgCHA, and (c) O_2-AgCHA.

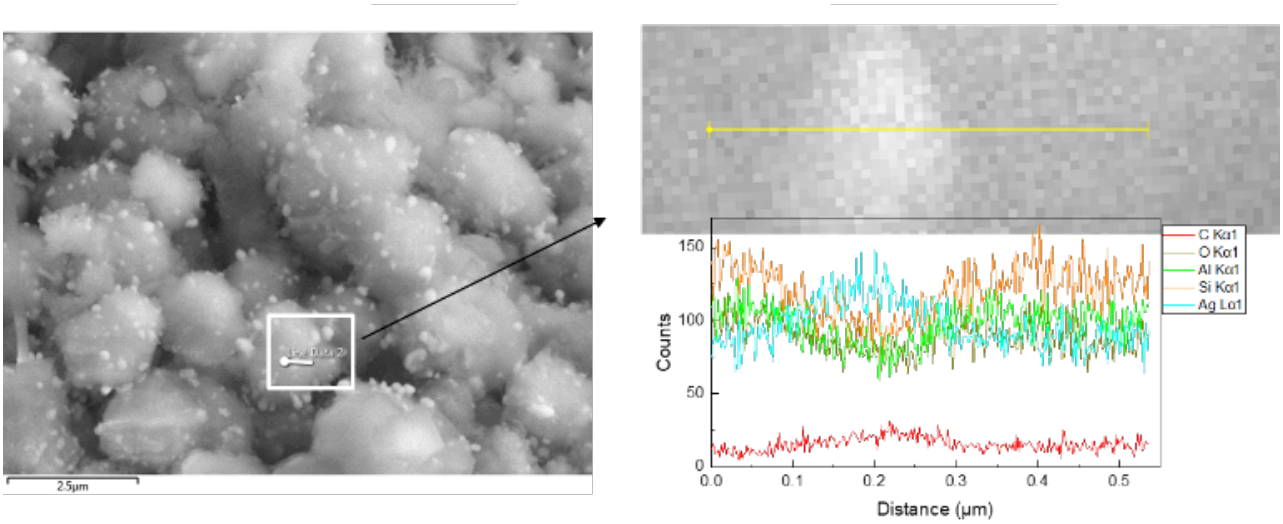

Figure 7. SEM/EDX scan of silver particles on the surface of the zeolite

The zeolite structure before and after reduction was evaluated using p-XRD in Figure 8. The p-XRD spectrum of H_2-AgCHA contained the main diffraction peaks for metallic silver, which was not observed in AgCHA sample alone. This is consistent with previous reports, where silver diffraction peaks only appear after hydrogen reduction due to the formation of larger silver particles under hydrogen exposure.[27] After reoxidation, the intensity of the silver peaks for O_2-AgCHA decreased significantly, indicating the formation of metallic silver is reversible. The O_2-AgCHA sample still contains a small amount of silver, as indicated by the presence of the Ag(111) peak. This is consistent with the thermodynamic measurements that showed a small decrease in Xe adsorption affinity for the O_2-AgCHA sample compared to the AgCHA; however, this may be further increased with increased oxidation.

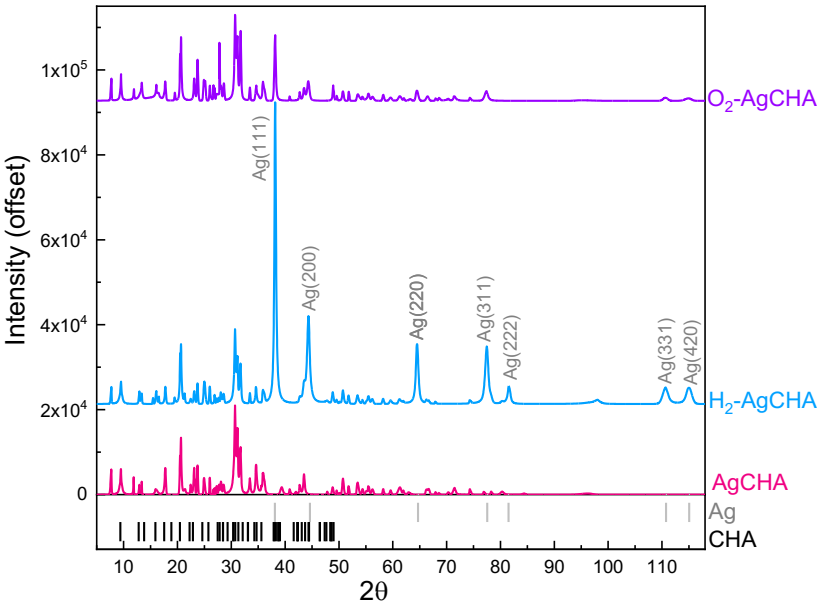

Figure 8. Effect of reduction and re-oxidation on p-XRD spectra. Peaks for metallic silver are labelled in gray.

Changes in the silver oxidation state was measured using XPS. As shown in Figure 9 and Table 4, reduction led to a ~1 eV negative shift in the binding energy for both Ag3d peaks. Peak deconvolution shows the presence of a small Ag signal close to the Ag binding energy for the AgCHA sample. Etching the Ag-CHA sample did not show a change in peak location; however, a positive peak shift was observed for H_2-AgCHA. Deeper etching removed the small shoulder peak due to the formation of nanoparticles on the surface that lead to a shift in the binding energy (Figure S4 and S5 and Table S2). Even at the deeper etch, there is still a negative shift in the binding energy for the reduced sample compared to the Ag-CHA and O_2-AgCHA. The smaller shift of 0.5-1 eV may point toward Ag^+ species rather than Ag^{2+}, which generally show larger peak shifts, about 2 eV. The atomic composition of the samples did not show a significant difference in relative oxygen content. XPS may not be sensitive enough to detect small changes to oxygen content bound to Ag (i.e. for Ag_2O vs AgO) since the Ag comprises about 2 atomic percent, much lower than the composition of oxygen in the zeolite (Table S3).

Etching the AgCHA sample did not change the Ag3d binding energy, indicating that the silver oxidation state is the same on the surface and in the pores (Figure S4), unlike in the H_2-AgCHA sample. The shift in Ag binding energy was reversible after re-oxidation and returned to the same oxidation state as the AgCHA. This indicates that the oxidation state is reversible and oxidation of the H_2-AgCHA sample recovered the original oxidation state. The shift of the binding energy correlated to a decrease in Xe binding, indicating that ionic silver is responsible for strong Xe adsorption in zeolites.

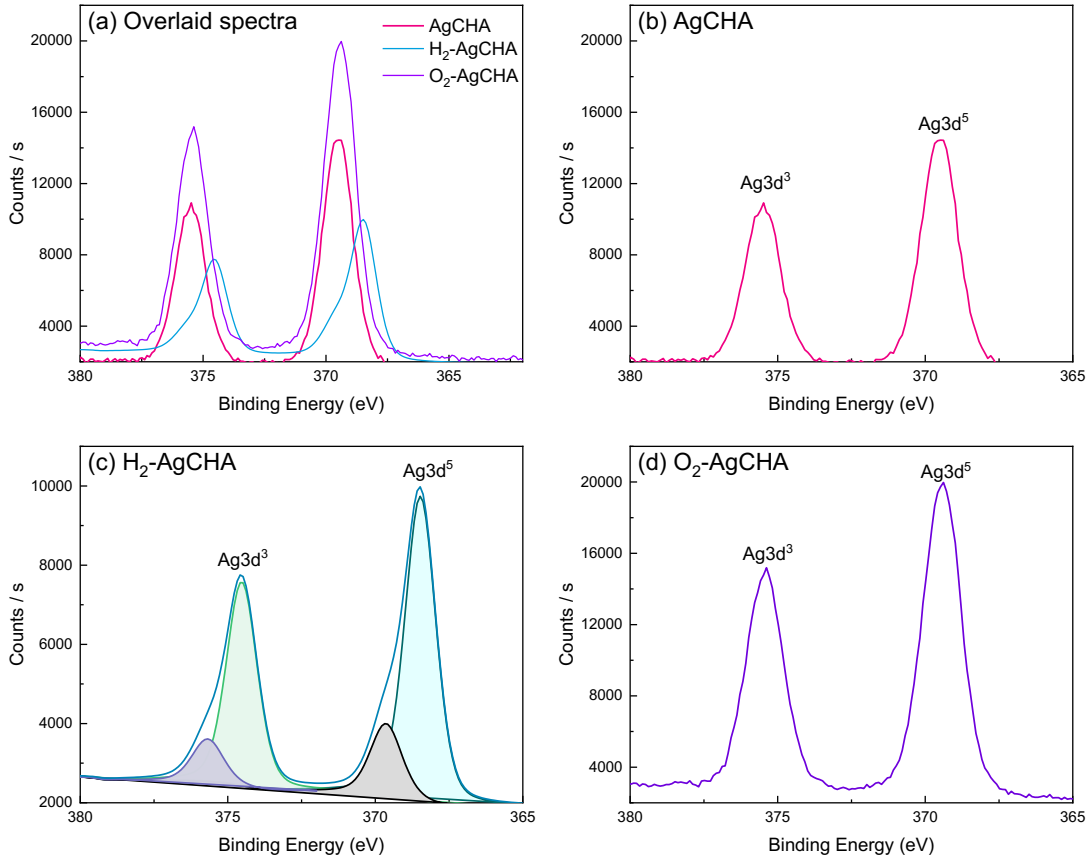

Figure 9. XPS results for (a) all spectra overlaid, (B) AgCHA, (c) H_2-AgCHA and (d) O_2-AgCHA

Table 4. Ag3d binding energy (BE) for the XPS data in Figure 9

Sample	**Ag 3d³ BE (ev)**	**Ag 3d⁵ BE (ev)**
AgCHA	375.5	369.5
H_2-AgCHA	374.52, 375.68	368.47, 369.52
O_2-AgCHA	375.42	369.43

This systematic investigation shows the adsorption of Xe is sensitive to the silver oxidation state. Even in the presence of silver nanoparticles, Xe adsorption was more favorable than the sample

without silver (CHA). The nature of adsorption, (i.e. physisorption, bonding through dπ-dπ back-donation or via σ donation from the 5p orbital of Xe to the 5s orbital of Ag) is most likely a result of the state of the silver at the time of the adsorption. The ability to tune the adsorption strength can lead to the creation of better sorbents for detection or gas purification or utilized for sorbent regeneration and recycling.

CONCLUSIONS

This data indicates that the silver ion plays a strong role in the binding of Xe during adsorption, where reduced silver negatively affects the binding of Xe to the zeolite. The thermodynamics of Xe adsorption onto Ag-CHA was investigated to elucidate the role of silver oxidation state on noble gas adsorption. The reduction of Ag-CHA decreased the strength of interaction of Xe adsorption and reoxidation recovered most of the binding strength. The freshly exchanged Ag-CHA had the strongest binding to Xe. Reduction by H_2 to create (H_2-AgCHA) lowered the heat of adsorption assumedly by converting Ag^+ to Ag^0. Re-oxidation recovered ~95% of the original binding strength. After reduction, silver nanoparticles were observed on the surface, as measured on p-XRD and SEM/EDS. A reversible shift in the Ag BE was observed in XPS for the re-oxidized sample.

ASSOCIATED CONTENT

Supporting Information.

Temperature programmed reduction and desorption experiments of different zeolites, effect of xenon concentration on retention time and additional XPS data

AUTHOR INFORMATION

Corresponding Author

*Kaitlin.Lawrence@entegris.com

Present Addresses

† 7 Commerce Rd, Danbury CT 06804

Author Contributions

The manuscript was written through contributions of all authors. All authors have given approval to the final version of the manuscript.

ACKNOWLEDGMENT

This work was supported by the Defense Threat Reduction Agency (DTRA) under Interagency Agreement number DTRA13081-38811. This work was produced by Battelle Savannah River Alliance, LLC under Contract No. 89303321CEM000080 and/or a predecessor contract with the U.S. Department of Energy. Publisher acknowledges the U.S. Government license to provide public access under the DOE Public Access Plan (http://energy.gov/downloads/doe-public-access-plan)

REFERENCES

1. P. E. Dresel, K. B. Olsen, J. C. Hayes, J. I. McIntyre, S. R. Waichler and B. M. Kennedy, Environmental applications of stable xenon and radioxenon monitoring, *J. Radioanal. Nucl.Chem.*, 2008, 276, 763-769.

2. A. Ringbom, T. Larson, A. Axelsson, K. Elmgren and C. Johansson, SAUNA–a system for automatic sampling, processing, and analysis of radioactive xenon. *Nucl. Instrum. Meth. A*, 2003, 508, 542-553.

3. N. P. Franks, R. Dickinson, S. L. M. de Sousa, A. C. Hall and W. R. Lieb, How does xenon produce anaesthesia? *Nature*, 1998, 396, 324-324.

4. K. Abe, J. Hosaka, T. Iida, M. Ikeda, *et. al*, Distillation of liquid xenon to remove krypton, *Astropart. Phys.*, 2009, 31, 290-296.

5. J. B. Robertson, Behavior of xenon-123 gas after injection underground: Molecular diffusion, materials balance, and barometric effects, *Report* 69-226, 1969.

6. C. R. Carrigan, R. A. Heinle, G. B. Hudson, J. J. Nitao and J. J. Zucca, Trace gas emissions on geological faults as indicators of underground nuclear testing, *Nature*, 1996, 382, 528-531.

7. Z. Wang, L. Bao, X. H. Hao, Y. L. Ju, K. Pushkin and M. He, Large scale xenon purification using cryogenic distillation for dark matter detectors, *J. Instrum.*, 2014, 9, P11024-P11024.

8. S. Kitani and J. Takada, Adsorption of Krypton and Xenon on Various Adsorbents, *J.Nucl. Sci. Technol.*, 1965, 2, 51-56.

9. T. T. P. Cheung, C. M. Fu and S. Wharry, Xenon-129 NMR of xenon adsorbed in Y zeolites at 144 K, *J. Phys. Chem.*, 1988, 92, 5170-5180.

10. R. Grosse, R. Burmeister, B. Boddenberg, A. Gedeon and J. Fraissard, Xenon-129 NMR of silver-exchanged X- and Y-type zeolites, *J. Phys. Chem.*, 1991, 95, 2443-2447.

11. R. Grosse, A. Gedeon, J. Watermann, J. Fraissard and B. Boddenberg, Adsorption and ^{129}Xe NMR of xenon in silver-exchanged Y zeolites: Application to the location of silver cations, *Zeolites*, 1992, 12, 909-915.

12. J. Watermann and B. Boddenberg, Isosteric heats of adsorption of xenon in silver-exchanged Y zeolites, *Zeolites*, 1993, 13, 427-429.

13. S. M. Kuznicki, A. Ansón, A. Koenig, T. M. Kuznicki, T. Haastrup, E. M. Eyring and D. Hunter, Xenon Adsorption on Modified ETS-10, *J. Phys. Chem. C.,* 2007, 111, 1560-1562.

14. H. G. Nguyen, G. Konya, E. M. Eyring, D. B. Hunter and T. N. Truong, Theoretical Study on the Interaction between Xenon and Positively Charged Silver Clusters in Gas Phase and on the (001) Chabazite Surface, *J. Phys. Chem. C*. 2009, 113, 12818-12825.

15. B. J. Sikora, C. E. Wilmer, M. L. Greenfield and R. Q. Snurr, Thermodynamic analysis of Xe/Kr selectivity in over 137 000 hypothetical metal–organic frameworks, *Chem. Sci.,* 2012, 3, 2217-2223.

16. C. Daniel, A. Elbaraoui, S. Aguado, M.-A. Springuel-Huet, A. Nossov, J.-P. Fontaine, S. Topin, T. Taffary, L. Deliere, Y. Schuurman and D. Farrusseng, Xenon Capture on Silver-Loaded Zeolites: Characterization of Very Strong Adsorption Sites, *J. Phys. Chem. C.,* 2013, 117, 15122-15129.

17. L. Deliere, S. Topin, B. Coasne, J.-P. Fontaine, S. De Vito, C. Den Auwer, P. L. Solari, C. Daniel, Y. Schuurman and D. Farrusseng, Role of Silver Nanoparticles in Enhanced Xenon Adsorption Using Silver-Loaded Zeolites, *J. Phys. Chem. C*., 2014, 118, 25032-25040.

18. L. Deliere, B. Coasne, S. Topin, C. Gréau, C. Moulin and D. Farrusseng, Breakthrough in Xenon Capture and Purification Using Adsorbent-Supported Silver Nanoparticles, *Chem. Eur. J*., 2016, 22, 9660-9666.

19. C. M. Simon, R. Mercado, S. K. Schnell, B. Smit and M. Haranczyk, What Are the Best Materials To Separate a Xenon/Krypton Mixture?, *Chem. Mater*., 2015, 27, 4459-4475.

20. H. S. Cho, K. Miyasaka, H. Kim, Y. Kubota, *et. al*, Study of Argon Gas Adsorption in Ordered Mesoporous MFI Zeolite Framework, *J. Phys. Chem. C*., 2012, 116, 25300-25308.

21. J. Sebastian and R. V. Jasra, Anomalous adsorption of nitrogen and argon in silver exchanged zeolite A, *Chem. Comm*. 2003, 268-269.

22. C. J. Jameson, A. K. Jameson and H. M. Lim, Competitive adsorption of xenon and krypton in zeolite NaA: 129Xe nuclear magnetic resonance studies and grand canonical Monte Carlo simulations, *J. Chem. Phys*. 1997, 107, 4364-4372.

23. B. J. Riley, J. D. Vienna, D. M. Strachan, J. S. McCloy and J. L. Jerden, Materials and processes for the effective capture and immobilization of radioiodine: A review, *J. Nucl. Mater.*, 2016, 470, 307-326.

24. C. G. Saxton, A. Kruth, M. Castro, P. A. Wright and R. F. Howe, Xenon adsorption in synthetic chabazite zeolites, *Microporous Mesoporous Mater.*, 2010, 129, 68-73.

25. I. L. Moudrakovski, C. I. Ratcliff and J. A. Ripmeester, 129Xe NMR Study of Adsorption and Dynamics of Xenon in AgA Zeolite, *J. Am. Chem. Soc.*, 1998, 120, 3123-3132.

26. S. T. Meek, S. L. Teich-McGoldrick, J. J. Perry, J. A. Greathouse and M. D. Allendorf, Effects of Polarizability on the Adsorption of Noble Gases at Low Pressures in Monohalogenated Isoreticular Metal–Organic Frameworks, *J. Phys. Chem. C.*, 2012, 116, 19765-19772.

27. T. Baba, N. Akinaka, M. Nomura and Y. Ono, Reversible interconversion of silver cations and silver metal particles in Ag-Y zeolite, *J. Chem. Soc. Chem. Commun.*, 1992, 339-340.

28. T. Sun and K. Seff, Silver Clusters and Chemistry in Zeolites, *Chem. Rev.*, 1994, 94, 857-870.

29. J. A. Widegren and T. J. Bruno, Enthalpy of adsorption for hydrocarbons on concrete by inverse gas chromatography, *J. Chromatogr. A*, 2011, 1218, 4474-4477.

30. S. Mohammadi-Jam and K. E. Waters, Inverse gas chromatography applications: A review, *Adv. in Colloid Interface Sci.*, 2014, 212, 21-44.

31. R. Ho and J. Y. Y. Heng, A Review of Inverse Gas Chromatography and its Development as a Tool to Characterize Anisotropic Surface Properties of Pharmaceutical Solids, *KONA Powder Part. J*, 2013, 30, 164-180.

32. M. Calligaris, G. Nardin and L. Randaccio, Cation site location in hydrated chabazites. Crystal structure of potassium- and silver- exchanged chabazites, *Zeolites*, 1983, 3, 205-208.

33. F. Chen, Y. Liu, R. E. Wasylishen, Z. Xu and S. M. Kuznicki, Solid-State NMR and TGA Studies of Silver Reduction in Chabazite, *J. Nanosci. Nanotechnol.*, 2012, 12, 1988-1993.

34. Y. Liu, F. Chen, S. M. Kuznicki, R. E. Wasylishen and Z. Xu, A Novel Method to Control the Size of Silver Nanoparticles Formed on Chabazite, *J. Nanosci. Nanotechnol.*, 2009, 9, 2768-2771.

35. T. L. Brown, H. E. LeMay, B. E. Bursten, C. J. Murphy, P. M. Woodward and M. W. Stoltzfus, *Chemistry: The Central Science*, Pearson, Upper Saddle River, NJ, 13th edn., 2015.

Table of Contents Image

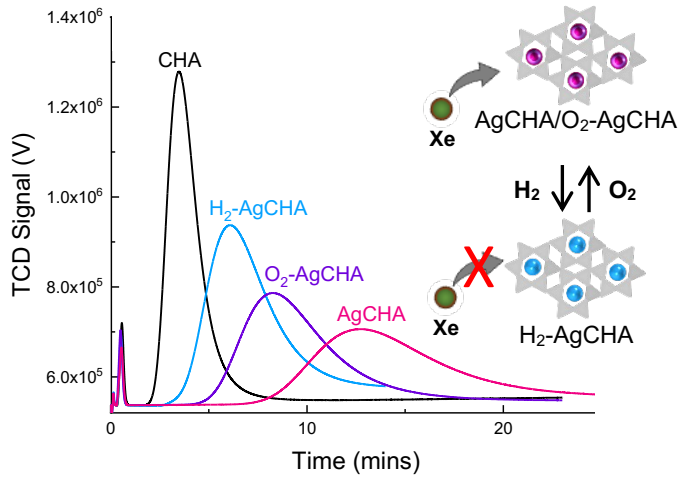

Supporting Information

Investigating the Role of Silver Oxidation State on the Thermodynamic Interactions between Xenon and Silver Functionalized Zeolites

Kaitlin J. Coopersmith,*[a] Katherine L. Broadwater,[a] Steven M. E. Demers,[a] Rebhadevi Monikandan,[b] Michael Torcivia,[a] Lindsay Roy,[a] and Douglas Hunter[a]

a. Savannah River National Laboratory, Aiken, SC 29808, United States
b. Materials Characterization Facility, Georgia Institute of Technology, Atlanta, Georgia 30332, United States

**Kaitlin.Lawrence@entegris.com*

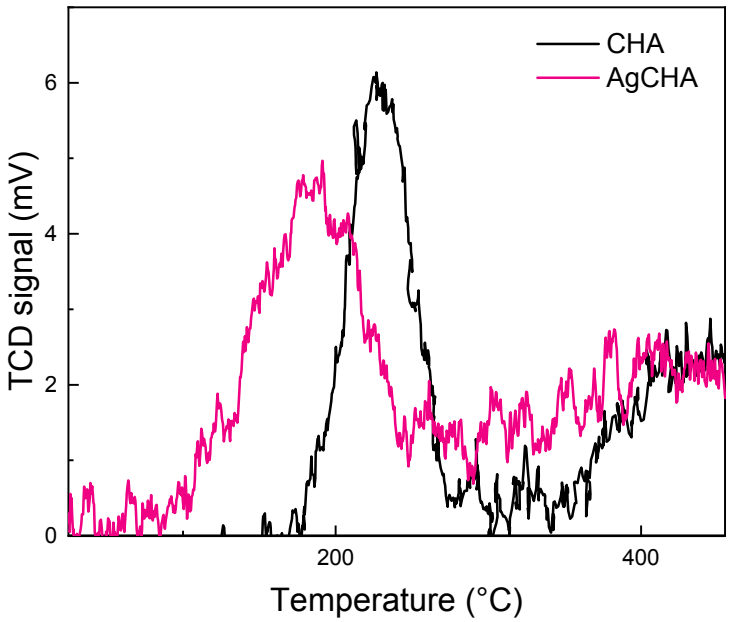

Figure S1. Temperature programmed reduction (TPR) of CHA and AgCHA. The carrier gas was a mixture of H_2 and He, so the consumption of H_2 should lead to an increase in the signal of the TCD since H_2 has a higher thermal conductivity. The standard reduction potential of silver (E^0=0.8 V) is higher than that of SiO_2 and Al (**Error! Reference source not found.**) and is more likely to be reduced by hydrogen.[1] Additionally, any strongly bound surface water can be released as a product of this reduction reaction. The TPR for AgCHA occurs at 184 °C, which is lower than that for the CHA at 228 °C. The presence of silver decreased the reduction temperature of these samples. This is consistent with previous reports, where the TPR of silver on NaY zeolites showed a main reduction peak before 200 °C.[2]

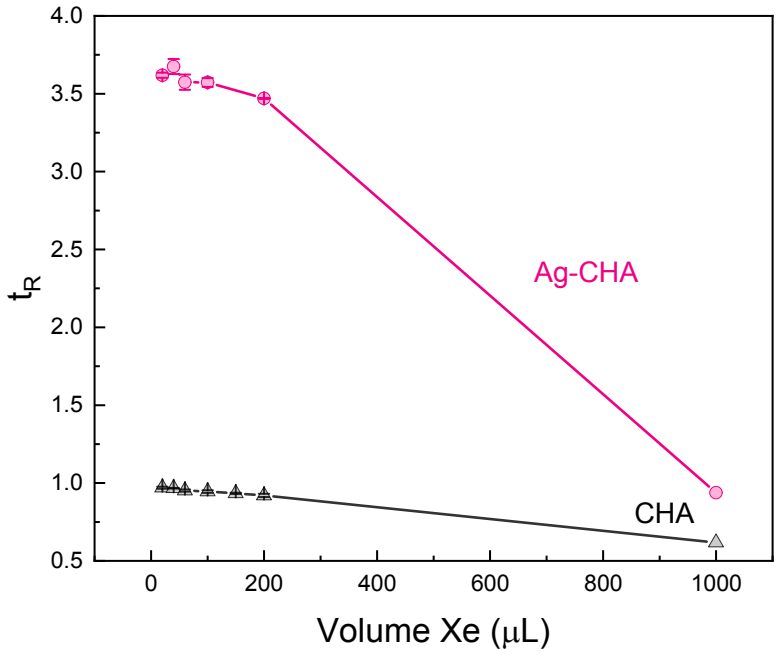

Figure S2. Effect of [Xe] on retention time for CHA and AgCHA. Xe volumes were chosen in the range where retention time was not dependent on volume within error. Error bars indicate standard deviation (1σ) of different Xe injections.

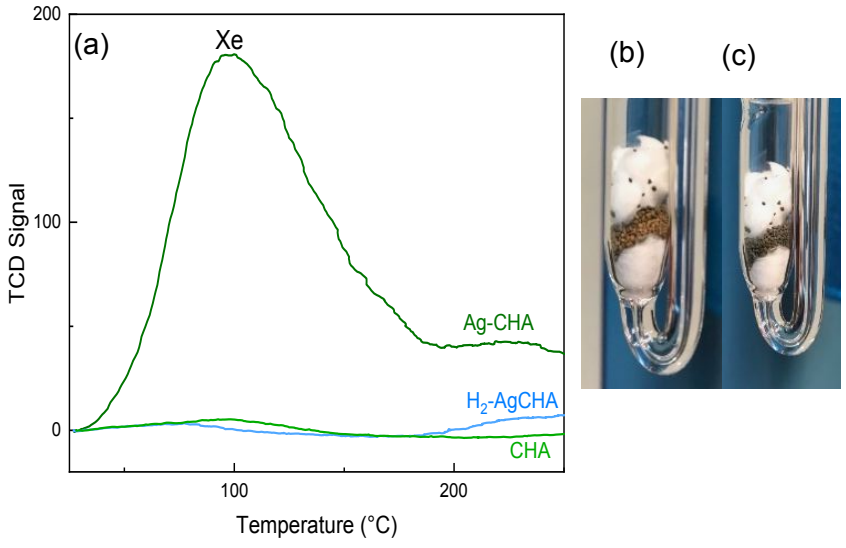

Figure S3. (a) TPD of Xe with different treatments for Ag-zeolites, (b) picture of zeolites in chemisorption cell before and (c) after reduction.

Table S1. Standard Reduction potentials in order of decreasing likelihood of reduction[1]	
Reaction	**E^0 (V)**
$O_2 + 4H + 4e^- \leftrightarrow 2H_2O$	1.229
$½\ H_2 + {}^-OH \leftrightarrow H_2O + e^-$	0.82
$Ag^+ + e^- \leftrightarrow Ag(s)$	0.8
$2H + 2e^- \leftrightarrow H_2(g)$	0
$SiO_2 + 4H^+ + 4e^- \leftrightarrow Si + 2H_2O$	-0.909
$Al(OH)_4^- + 3e^- \leftrightarrow Al(s) + 4\ {}^-OH$	-2.31

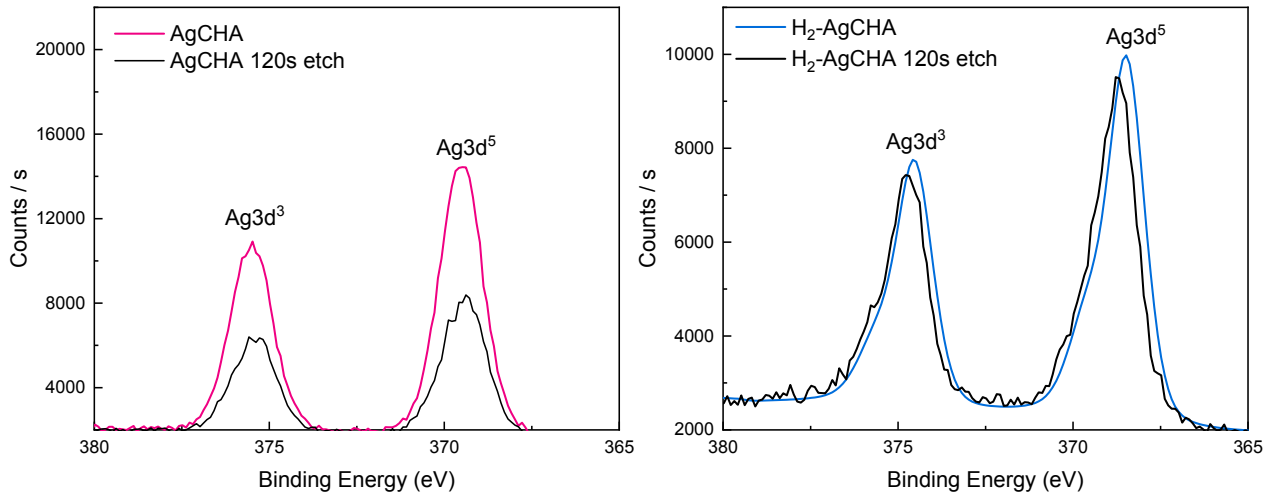

Figure S4. Effect of etching on XPS BE for Ag3d peaks for AgCHA and H_2-AgCHA after 120 s etch with 500 eV ion gun.

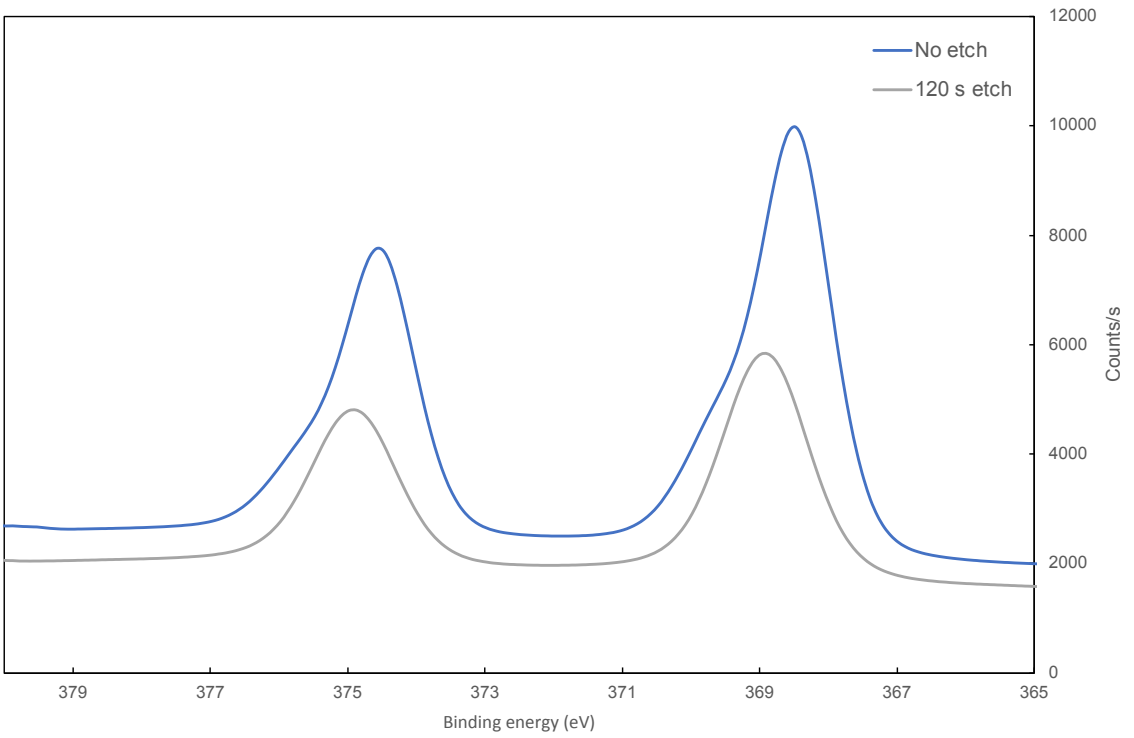

Figure S5. Deeper etch of H_2-AgCHA sample with 2000 eV electron gun and 120 s etch time.

Table S2. Binding energy for H_2-AgCHA with different etching		
Sample	**Ag $3d^3$ BE (ev)**	**Ag $3d^5$ BE (ev)**
No etch	374.52, 375.68	368.47, 369.52
500 eV, 120 s etch	374.72, 375.89	368.68, 369.79
2000 eV, 120 s etch	374.90	368.91

Table S3. Atomic Percent from XPS for each sample						
Sample	**O1s**	**Si 2p**	**Al2p**	**Ag3d**	**Si/Al**	**Ag/(Si+Al)**
CHA	66.8	24.6	8.6	0	2.9	0
Ag-CHA	61.8	26.1	8.8	3.3	3.0	0.09
H_2-AgCHA	64.1	25.8	8.3	1.8	3.1	0.05
O_2-AgCHA	62.6	26.3	8.0	3.0	3.3	0.09

References:

1. G. C. Milazzo, S.; Sharma, V. K., *Tables of Standard Electrode Potentials*, Wiley, London, 1978.

2. D. Chen, Z. Qu, S. Shen, X. Li, Y. Shi, Y. Wang, Q. Fu and J. Wu, *Catalysis Today*, 2011, **175**, 338-345.